JOURNAL OF THERMOPHYSICS AND HEAT TRANSFER
Vol. 24, No. 1, January–March 2010

# Durable Heat Flux Sensor for Extreme Temperature and Heat Flux Environments

Andrew R. Gifford,* David O. Hubble,* Clayton A. Pullins,* Thomas E. Diller,† and Scott T. Huxtable‡
*Virginia Polytechnic Institute and State University, Blacksburg, Virginia 24061*

DOI: 10.2514/1.42298

**This paper reports on the development and evaluation of a novel heat flux sensor, the high-temperature heat flux sensor, tested at temperatures and heat flux levels in excess of 1000°C and 10–13 $W/cm^2$, respectively. The current sensor configuration uses type-K thermocouple materials in a durable welded thermopile arrangement contained within a surface-mountable high-temperature housing. The steady-state sensitivity of the design is predicted using a simplified one-dimensional thermal-resistance model. The design performance of a prototype sensor is validated using both conduction and convection heat transfer calibration at low temperature. The average experimental values of the sensitivity are $623 \pm 33$ $mV/W/cm^2$ and $579 \pm 29$ $mV/W/cm^2$ in conduction and convection, respectively. These calibration results compare very well with the predicted room-temperature sensitivity of 559 $\mu V/W/cm^2$. Minimal dependence on heat transfer coefficient is found in convection. Prolonged thermal cycling of the sensor using a high-temperature kiln and a propane torch apparatus demonstrates survivability near the maximum temperature of the thermoelectric materials with negligible oxidation or loss of calibration.**

## Nomenclature

| | | |
|---|---|---|
| $a$ | = | surface area normal to the principle direction of heat transfer |
| $B_e$ | = | bias error |
| $h$ | = | heat transfer coefficient |
| $k$ | = | thermal conductivity |
| $N$ | = | number of thermoelectric element pairs |
| $n$ | = | number of sensor components |
| $P_e$ | = | precision error |
| $q''$ | = | heat flux |
| $R''$ | = | thermal resistance |
| $S$ | = | sensor sensitivity |
| $S_{AB}$ | = | Seebeck coefficient for thermoelectric elements A and B |
| $T$ | = | temperature |
| $t_s$ | = | thermal response time |
| $U$ | = | measurement uncertainty |
| $V$ | = | thermoelectric output voltage |
| $X_i$ | = | $i$th independent measurement variable |
| $\alpha$ | = | thermal diffusivity |
| $\delta$ | = | thickness in the principle direction of heat transfer |

*Subscripts*

| | | |
|---|---|---|
| $A$ | = | thermoelectric element A |
| $B$ | = | thermoelectric element B |
| cond | = | conduction |
| conv | = | convection |
| ins | = | insulation |
| $j$ | = | heated air jet |
| ref | = | reference sensor |
| $t$ | = | HTHFS sensor |
| $W$ | = | weld |

Received 20 November 2008; revision received 30 April 2009; accepted for publication 30 April 2009. 

*Ph.D. Candidate, Mechanical Engineering, Advanced Experimental Thermofluid Engineering Research Laboratory. Student Member AIAA.

†Professor, Mechanical Engineering, Advanced Experimental Thermofluid Engineering Research Laboratory. Member AIAA.

‡Assistant Professor, Mechanical Engineering. Member AIAA.

## I. Introduction

THE measurement of heat flux in extreme environments is a challenging task. Take, for instance, the high-temperature turbulent flow environments found in modern turbomachinery or the searing temperatures, high heating rates, and aerodynamic loads on a spacecraft thermal protection system. Measurement of heat flux in these conditions is notoriously difficult because most sensors have trouble surviving long enough to provide useful and cost-effective engineering data [1]. Recently, the high-temperature heat flux sensor (HTHFS) was prototyped and characterized to address the difficulty in making accurate long-duration heat flux measurements under these types of conditions [2]. The focus of the current study is to detail the design and performance of the HTHFS.

## II. Heat Flux Sensor Design and Manufacture

The current version of the HTHFS design is shown schematically in Fig. 1. The heat flux sensor is composed of alternating thermoelectric element pairs connected electrically in series with electrical insulators isolating each element. The thermoelectric elements are precision-cut to a tolerance of approximately $\pm 0.001$ in. using a low-speed dicing saw. This ensures accurate sensor thickness for repeatability in manufacturing and calibration. Construction of the sensor is performed using a resistance welding technique that makes the thermopile simple and robust. As shown in Fig. 1, the thermopile is set securely in a high-temperature metal housing with insulating potting material to create smooth mounting surfaces. Four bolts may be used in conjunction with thermal adhesive to flush-mount and secure the sensor to the measurement surface. Two thermocouples are welded to either end of the sensor thermopile to measure the top and bottom surface temperatures as well as the differential voltage generated by the thermopile, which corresponds to heat flux. These wires are routed through the housing into thermally shielded strain-relieved extension wires that carry the signals safely to a data acquisition (DAQ) system or other voltage-sensing device.

When the HTHFS is affixed properly to a measurement surface, any heat flux applied to the surface will result in a temperature gradient across the effective thermal resistance of the thermopile. The temperature gradient serves to generate a voltage that may be calibrated directly to the amount of applied heat flux. The voltage output (sensitivity) is scalable based on the number of thermoelectric element pairs and the Seebeck coefficient of each thermoelectric element pair. The novel use of the thermopile as the

**Table 1 Thermocouple material properties: maximum temperatures**

| Metal/alloy | Solidus/melt, °C |
|---|---|
| Alumel | 1398 |
| Copper | 1085 |
| Constantan | 1171 |
| Chromel | 1426 |
| Nickel | 1452 |
| Palladium | 1553 |
| Platinum | 1768 |
| Platinum/15% iridium | 1552 |
| Platinum/13% rhodium | 1771 |
| Platinum/1% rhodium | 1771 |
| Platinum/5% molybdenum | 1770 |
| Platinum/0.1% molybdenum | 1770 |

**Table 2 Thermocouple material properties: Seebeck coefficients near room temperature**

| Element A | Element B | $S_{AB}$, $\mu$V/°C |
|---|---|---|
| Constantan | Alumel | 34.0 |
| Chromel | Alumel | 40.0 |
| Constantan | Copper | 39.4 |
| Nickel | Copper | 22.1 |
| Platinum | Copper | 6.70 |
| Chromel | Constantan | 60.1 |
| Nickel | Constantan | 20.5 |
| Platinum | Constantan | 35.9 |
| Platinum | Nickel | 15.4 |
| Platinum/15% iridium | Palladium | 26 |
| Platinum/13% rhodium | Platinum/1% rhodium | 6 |
| Platinum/5% molybdenum | Platinum/0.1% molybdenum | 20 |

thermal-resistance layer is the fundamental difference between the HTHFS and most differential heat flux sensors that have been developed over the years [1]. Traditional differential heat flux sensors use a separate thermal-resistance layer to create a temperature drop across the sensor. The temperature gradient is measured separately using thermocouples or resistance-temperature detectors. This leads to added complexity and cost and, in some cases, decreased reliability.

A review of potential thermoelectric alloys was completed before constructing the high-temperature version of the HTHFS. The results are tabulated in Tables 1 and 2 [3–5]. It is clear in examining Table 1 that a wide variety of HTHFS configurations are possible with extremely high operating temperatures. Standard type-K (Chromel P® and Alumel®) materials were used for the current sensor, due mainly to the high Seebeck coefficient, high-temperature rating (greater than 1000°C), durability, and relatively low cost.

The electrical insulator, which is sandwiched between the thermoelectric elements, has to provide the same high-temperature capability, with a particular emphasis on survivability under thermal stress. A survey of potential insulators was completed, with preference given to fire-cured ceramic pastes and thin ceramic plates composed primarily of aluminum oxide.

Because the sizes of the thermopile and electrical insulators are arbitrary, the HTHFS may also be scaled down to provide high frequency response, which is essential to capture transient events such as shock wave passage or freestream–turbulence interactions. The current HTHFS size is $9.0 \times 7.0 \times 3.1$ mm (length by width by height). An acceptable estimate of the 95% thermal time response $t_s$ for a surface-mounted heat flux sensor with a proper heat sink is given by Hager [6] as a ratio of sensor thickness $\delta_t$ squared and the effective thermal diffusivity of the sensor $\alpha$:

$$t_s = 1.5\delta_t^2/\alpha \tag{1}$$

Using the thermal properties and size of the current HTHFS, a thermal response time of roughly 2 s is obtained. This gives a frequency response on the order of 0.5 Hz. Although this is considered to be too low for capturing fast transients, it is clear that only a modest decrease in the thickness of the sensor can greatly increase the frequency response.

## III. Theoretical HTHFS Sensitivity

Prediction of the sensitivity of the HTHFS is based on a simple heat transfer analysis using Fourier's law and a thermal-resistance model. Prediction of the sensitivity requires mathematical expressions for the voltage generated across the sensor under operating conditions, along with the heat flux through the sensor.

As shown in Fig. 2, the sensor consists of $n_A$ and $n_B$ thermoelectric elements in a thermopile arrangement, creating an even number of $N = [(n_A - 1) + n_B]/2$ pairs. For this particular HTHFS design, there is an extra piece of element A welded to the right-hand side of the sensor that facilitates attachment of the thermocouple lead wires shown in Fig. 1. Note that the extra element does not contribute to the thermoelectric output of the thermopile, because it is essentially an extension of the thermocouple lead wire; however, its presence does add to the overall thermal resistance of the sensor. With an applied heat flux, a temperature gradient $\Delta T = (T_2 - T_1)$ exists across the thermal resistance $R_t''$ of the sensor elements. In this case, $T_2$ and $T_1$, respectively, are the top and bottom surface temperatures of the gauge. This temperature gradient generates a thermoelectric voltage $V_t$, which is calculated according to

$$V_t = NS_{AB}(T_2 - T_1) \tag{2}$$

where $S_{AB}$ is the Seebeck coefficient for the thermoelectric alloys used in this study. The heat flux through the sensor is

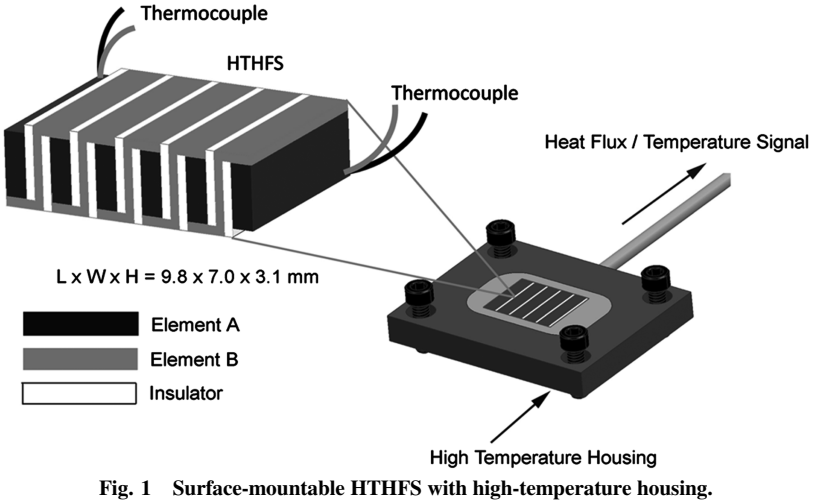


**Fig. 1 Surface-mountable HTHFS with high-temperature housing.**

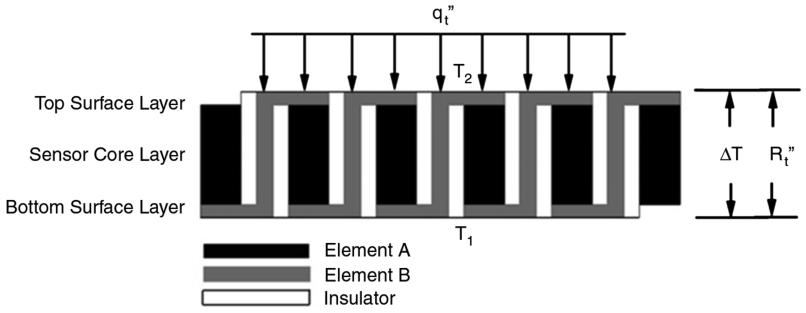


**Fig. 2 Principle of operation for HTHFS.**

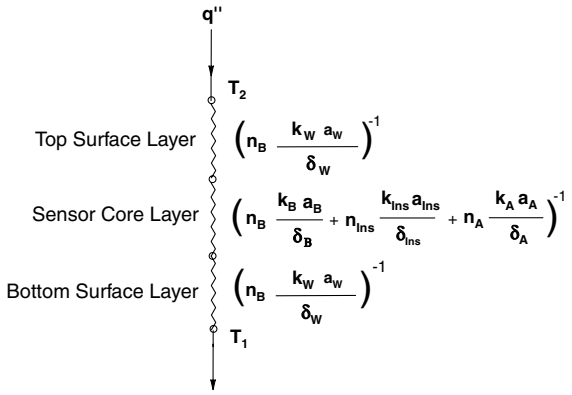


**Fig. 3 Simplified 1-D thermal-resistance model of HTHFS.**

$$q_t'' = (T_2 - T_1)/R_t'' \tag{3}$$

where $R_t''$ is the thermal resistance in the principle direction of heat transfer. Using the configuration of the HTHFS shown in Fig. 2, a simplified one-dimensional thermal-resistance model was constructed to estimate $R_t''$. The resulting model is shown in Fig. 3. In this model, the variables $k$, $a$, and $\delta$ are the thermal conductivity, surface area, and thickness in the principal direction of heat transfer for each element, respectively. The subscripts $A$, $B$, $t$, ins, and $W$ are used to denote element A, element B, HTHFS, insulation, and weld, respectively. The thermal-resistance model consists of three distinct layers situated in series across the thickness of the HTHFS. Isothermal surfaces are assumed on the top and bottom surfaces and between each layer. Given the HTHFS materials and design, it is assumed that parallel conduction is dominant in all three layers, with adiabatic boundaries between elements. The resulting overall thermal resistance is

$$R_t'' = a_t(n_A(k_A a_A/\delta_A) + n_{\text{ins}}(k_{\text{ins}} a_{\text{ins}}/\delta_{\text{ins}}) + n_B(k_B a_B/\delta_B))^{-1} + 2a_t(n_B k_W a_W/\delta_W)^{-1} \tag{4}$$

Finally, the theoretical sensitivity for the HTHFS is found by division of Eq. (2) by Eq. (3):

$$S_{t-\text{cond}} = V_t/q_t'' = NS_{AB}R_t'' \tag{5}$$

Using Eq. (4) the calculated value of the thermal resistance for the sensor evaluated in this study is $R_t'' = 2.78\ \text{cm}^2 \cdot {}^\circ\text{C/W}$, where room-temperature thermal properties are used for each sensor component. It follows from Eq. (5) that the theoretical conduction sensitivity of the HTHFS sensor is $S_{t-\text{cond}} = 559\ \mu\text{V/W/cm}^2$.

## IV. Heat Flux Sensor Calibration

### A. Introduction

The measurements obtained from a heat flux sensor are only as accurate as the method used in the sensor's calibration. The substitution method of heat flux calibration is to apply a repeatable reference heat flux to both the test sensor to be calibrated and a reference sensor. The reference standard is assumed to accurately measure the reference heat flux. Sensitivity for the test sensor is obtained by simply dividing its voltage output by the heat flux measured by the reference sensor. The heat flux through the test and reference gauges may be due to radiation, convection, conduction, or mixed modes of heat transfer. It has been shown that the most useful calibration results are obtained when calibration is performed using the mode(s) of heat transfer that the sensor will experience in actual use [1]. The HTHFS sensor used in this study was first calibrated in conduction as a means of validating the analytical sensitivity calculations. The sensor was then calibrated in convection, because this mode of heat transfer will be important in many of the proposed applications for the HTHFS. Note that in this study the sensor temperatures and applied heat flux levels for both calibration approaches range from 60–80°C and 1–1.5 $\text{W/cm}^2$, respectively. Therefore, the results are only valid for low temperatures and heat flux levels. Calibrations to determine the sensitivity behavior of the HTHFS at higher temperature and higher heat flux levels will be addressed in future studies.

### B. Conduction Calibration

A new conduction calibration facility was recently developed in the Advanced Experimental Thermofluid Engineering Research (AEThER) laboratory at Virginia Polytechnic Institute and State University to complement existing convection calibration facilities for shear and stagnation flow, which are detailed in a work by Gifford et al. [7]. The core of the conduction calibration facility is shown schematically in Fig. 4.

The conduction calibration facility is designed to supply a uniform heat flux through both the HTHFS sensor and a reference heat flux sensor. As shown in Fig. 4, a uniform heat flux is supplied by a thin-film resistance heating element encased in two high thermal conductivity aluminum plates. The desired level of heat flux is set by a precision voltage regulator. Heat fluxes from 0.1–1.5 $\text{W/cm}^2$ are available with this heating element. Thermal energy is carried out of the system using an internally-water-cooled aluminum chamber. Chilled water is circulated through the chamber using a high-flow-rate pump submerged in an ice bath. A uniform heat flux is maintained through the HTHFS layer by surrounding the sensor with a metal mask made of material similar to the HTHFS housing material. A mask is also used around the reference heat flux sensor of similar composition and thickness. An RdF Corporation Micro-Foil® heat flux sensor is used as the reference sensor in the conduction calibration facility. Contact resistance is minimized to a uniform level between the heated surface and the HTHFS as well as the cooled surface and the reference sensor via conformable layers of Gap Pad®. The interface between the reference and HTHFS sensors is filled with a thermal grease to fill in asperities and minimize contact resistance. Two hardened-steel plates are positioned on the top and bottom of the stack to ensure repeatable calibration results. An equal torque applied to four bolts in the steel plates draws the stack together to create constant clamping pressure through the stack. Heat transfer to the steel plates is minimized by high-density insulating plates. Likewise, heat transfer via radiation and free convection from the sides of the stack is minimized by tightly packed, low-thermal-conductivity, fibrous insulation (not shown).

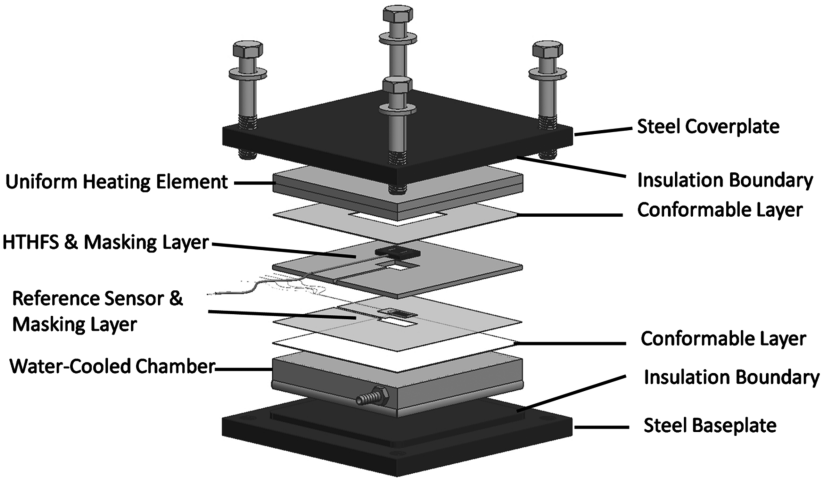


**Fig. 4 The core of the conduction calibration facility.**

Instrumentation of the conduction calibration facility includes thermocouples as well as the lead wires carrying the voltage signals from the HTHFS and reference heat flux sensors. Type-K thermocouples are used to monitor both the heater core temperature and the water temperature, which helps to ensure that steady-state conditions are achieved before taking heat transfer data. The HTHFS and the reference sensor have built-in thermocouples for sensor temperature monitoring. All signals are recorded directly using a 24-bit National Instruments DAQ system connected to a PC. No amplification of the signals is necessary. All channels are sampled at 1 Hz because only steady-state heat transfer information is desired. Data are post-processed in MATLAB. The time-averaged experimental conduction sensitivity $\overline{S_{t-\text{cond}}}$ for the HTHFS is calculated using the following equation once steady-state conditions are achieved:

$$\overline{S_{t-\text{cond}}} = \frac{V_t}{V_{\text{ref}}/S_{\text{ref}}} \tag{6}$$

where $V_t$ is the output voltage for the HTHFS, $V_{\text{ref}}$ is the output voltage from the reference sensor, and $S_{\text{ref}}$ is the sensitivity of the reference heat flux sensor. The time interval used for averaging was 60 s.

In this study, three series of conduction calibrations were performed consisting of four repeated trials each. For each series of four trials, the HTHFS was mounted in the conduction calibration facility with new conformable layers and thermal grease and compressed to the same stack pressure. Although the main goal of the conduction calibrations was to validate the analytical model predictions, the calibrations were also used to examine the effects of thermal cycling on conduction sensitivity. The first series of calibrations were performed on the HTHFS after repeated thermal cycling for extended periods of time at 1050°C in air within a high-temperature kiln. The second and third series of calibrations were performed on the same sensor after repeated thermal cycling with a propane torch. In this case, the sensor surface temperature approached 225°C, with the sensor measuring heat flux on the order of 10–13 W/cm$^2$. Details of the thermal cycling regiments with kiln and torch are found in Sec. V. Figure 5 shows the final conduction calibration results for the series of trials described previously.

As shown in Fig. 5, the conduction calibration results compare favorably with the theoretical sensitivity calculation given the assumptions made in the thermal-resistance model. The mean experimental sensitivity across all three series of calibrations is $S_{t-\text{cond}} = 623 \pm 33$ $\mu$V/W/cm$^2$, which is only 11.5% higher than the estimated theoretical sensitivity. Considering the minimal scatter in the experimental sensitivity from series to series, it is apparent that repeated thermal cycling with the kiln and the propane torch has only a minimal impact on HTHFS conduction sensitivity.

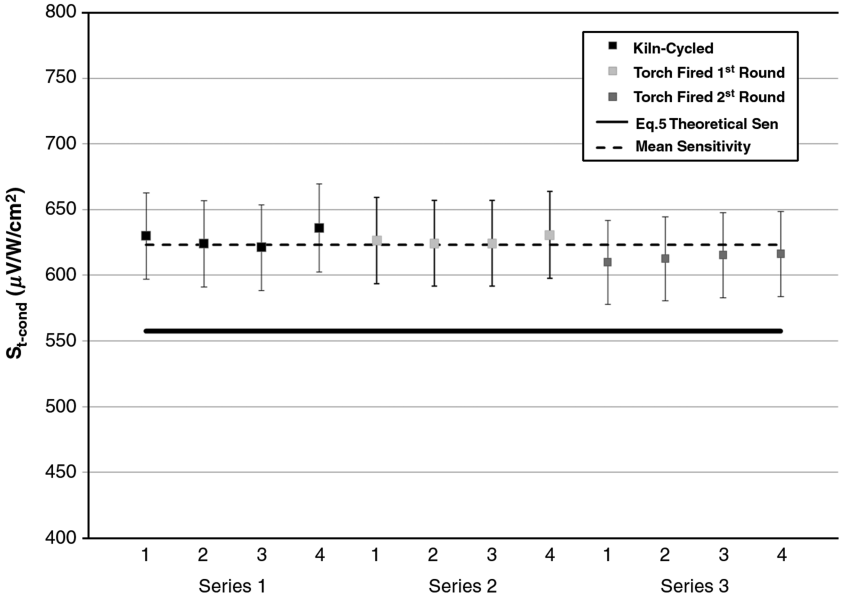


**Fig. 5 Conduction calibration results.**

### C. Convection Calibration

The HTHFS sensor used in this study was also calibrated in jet stagnation point flow in anticipation that it will be used heavily in engineering applications involving convective heat transfer. Calibrations were performed in the AEThER laboratory convection calibration facility after the thermal cycling. The design and performance of the convection calibration facility is detailed in a recent publication by Gifford et al. [7]. The core of the convection calibration facility is shown schematically in Fig. 6.

The stagnation flow convection calibration facility is composed of a main aluminum test stand, fully adjustable aluminum T-nozzle, and two sensor mounting plates. High-pressure heated air from a custom heat exchanger (not shown) is directed through the precision-machined T-nozzle, where it is split evenly and directed toward both a reference heat flux sensor and a test sensor. The turbulent heat transfer coefficient on each side of the T-nozzle is identical to within approximately 3% at the stagnation point [7]. A Vatell Corporation HFM-7® heat flux sensor is surface-mounted in the left-hand plate at the stagnation point. A press-fit type-K thermocouple measures plate surface temperature near the HFM-7. This provides the reference heat transfer coefficient for a particular test. A type-K thermocouple in the T-nozzle provides total temperature measurement of the jet before exiting the nozzle. At steady-state flow conditions, these measurements provide the heat transfer coefficient for a given air line pressure using Newton's law of cooling:

$$h = (V_{\text{ref}}/S_{\text{ref}})/(T_j - T_{\text{ref}}) \tag{7}$$

where $V_{\text{ref}}$ is the output voltage for the HFM-7, $S_{\text{ref}}$ is the sensitivity of the HFM-7 reference heat flux sensor, and $T_j - T_{\text{ref}}$ is the temperature difference between the T-nozzle and the HFM-7 surface.

On the right-hand side of the convection test stand, the standard calibration plate is replaced by a metal mask that holds the HTHFS sensor. This is similar to the mask used in the conduction calibration facility. Immediately behind the HTHFS is the same RdF Corporation Micro-Foil reference heat flux sensor used in the conduction calibration experiments. A water-cooled chamber with a smooth aluminum surface is placed behind this reference sensor to create a constant rear surface temperature. The chamber is cooled using a high-flow-rate pump submerged in an ice-water bath. The four mounting screws on the HTHFS housing are used to draw the HTHFS, Micro-Foil sensor, and water-cooling chamber tightly together. Thermal grease is used to minimize contact resistance. Under steady-state conditions the output voltage from the HTHFS coupled with the reference heat flux measurement from the RdF Micro-Foil sensor provides the experimental sensitivity for the HTHFS in convection as a function of heat transfer coefficient $h$. This is calculated in exactly the same fashion as the conduction calibration using Eq. (6). All signals are recorded and processed in the same fashion as conduction calibrations.

The results of the convection calibration are shown in Fig. 7. A total of four cases, consisting of four trials each at a particular line-pressure setting, were performed for the convection calibration. Despite increasing uncertainty in the heat transfer coefficient over the range of $h = 0.02$–$0.07\ \text{W/cm}^2 \cdot {}^\circ\text{C}$, the HTHFS sensitivity is essentially constant. Hence, sensitivity does not appear to depend on the heat transfer coefficient. The mean HTHFS sensitivity over the range of heat transfer coefficients is $S_{t-\text{conv}} = 579 \pm 29\ \mu\text{V/W/cm}^2$. The mean sensitivity is only around 4% higher than the theoretical sensitivity predicted via Eq. (5) for conduction and only 7.5% lower than the mean experimental conduction calibration sensitivity.

### D. Calibration Uncertainty Analysis

The following uncertainty analysis was performed on the calculation of the experimental sensitivity of the HTHFS in conduction and convection. The analysis follows that of Coleman and Steele [8]. The total uncertainty in the HTHFS sensitivity $S_t$ for a particular measurement is

$$\left(\frac{U_{S_t}}{S_t}\right)^2 = \sum_{i=1}^{J}\left(\frac{1}{S_t}\frac{\partial S_t}{\partial X_i}UX_i\right)^2 \tag{8}$$

where $U_{St}$ is the total experimental uncertainty, which is a function of independent experimental variables $X_i$. The total uncertainty in each independent variable is given by $U_{Xi}$, and $\partial St/\partial Xi$ are the associated sensitivity coefficients. Using the formula for the time-averaged experimental gauge sensitivity presented in Eq. (6) for conduction, the expanded form of Eq. (8) becomes

$$U_{S_t-\text{cond}} = S_t\sqrt{\left(\frac{1}{V_t}\right)^2 U_{V_t^2} + \left(\frac{-1}{V_{\text{ref}}}\right)^2 U_{V_{\text{ref}}^2} + \left(\frac{1}{S_{\text{ref}}}\right)^2 U_{S_{\text{ref}}^2} + U_{\text{rep}}} \tag{9}$$

where $U_{\text{rep}}$ is the estimated bias error in the repeatability of the conduction calibration facility. The conduction calibration facility repeatability uncertainty is estimated at $U_{\text{rep}} = 1.3\%$ of the measured sensitivity. Equation (9), with the exception of $U_{\text{rep}}$, is identical in form to that used for the convection calibration data. However, there is also an uncertainty associated with the measured heat transfer coefficient in the convection calibration experiments. Application of Eqs. (7) and (8) gives the following uncertainty in heat transfer coefficient:

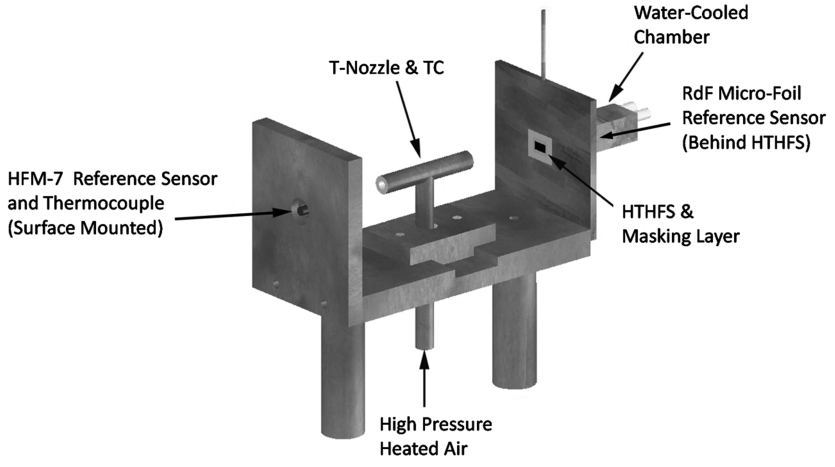


**Fig. 6 The core of the stagnation flow convection calibration facility (TC denotes thermocouple).**

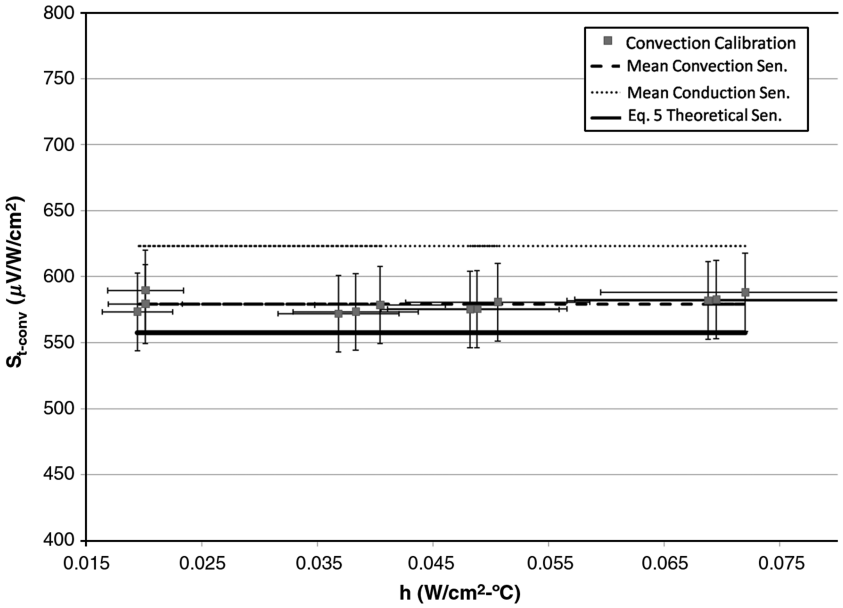


**Fig. 7 Convection calibration results.**

$$U_h = h\sqrt{\left(\frac{-1}{T_j - T_{\text{ref}}}\right)^2 U_{T_j^2} + \left(\frac{1}{T_j - T_{\text{ref}}}\right)^2 U_{T_{\text{ref}}^2} + \left(\frac{1}{V_{\text{ref}}}\right)^2 U_{V_{\text{ref}}^2} + \left(\frac{-1}{S_{\text{ref}}}\right)^2 U_{Sr^2} + U_{h-\text{SS}}} \tag{10}$$

In this case, uncertainty in the convection calibration stand $h$ value from side to side is $U_{h-\text{SS}} = 3\%$ of the measured heat transfer coefficient.

Uncertainties in each independent variable are estimated or calculated using each variable's precision and bias error limits according to Eq. (11):

$$U_{Xi} = \sqrt{B_{e-Xi}^2 + P_{e-Xi}^2} \tag{11}$$

Bias limits for the thermocouples used in the convection calibrations are a combination of thermocouple and data acquisition bias errors, and in this case depend on the mean values used to calculate the average sensitivity at a particular value of the heat transfer coefficient. A bias limit of 0.1°C is quoted with the DAQ, and a bias error of 0.75% of full scale is quoted for each thermocouple reading, giving

$$B_{e-Tj,\text{ref}} = \sqrt{(0.1)^2 + (0.0075\bar{T}_{j,\text{ref}})^2} \tag{12}$$

The precision limits were calculated from 128 continuous samples of nominal room-temperature data using Student's $t$-distribution with 127 degrees of freedom and a 95% confidence interval. Table 3 reports the overall average bias, precision, and total uncertainty in each measured quantity for the calibrations performed on the HTHFS in conduction and convection. All quantities are averaged over the number of experiments performed. Note that the reference sensor designations are written explicitly in Table 3 to avoid confusion.

The experimental conduction and convection sensitivities averaged over each series of trials are summarized in Table 4. The total uncertainty as a percentage of the overall sensor sensitivity is included. The percentage uncertainty is around 5% for the conduction calibrations and 5% for the convection calibrations. As apparent in Tables 3 and 4, the largest component of the total uncertainty for

**Table 3 Average bias, precision, and total uncertainties in measured and calculated variables**

| $X_i$ | Bias limit | Precision limit | Total | Units |
|---|---|---|---|---|
| | | *Conduction calibration* | | |
| $V_{\text{RdF}}$ | 3.92 | 1.67 | 4.26 | μV |
| $V_{\text{HTHFS}}$ | 3.92 | 1.14 | 4.08 | μV |
| $S_{\text{RdF}}$ | 46.25 | —— | 46.25 | μV/W/cm² |
| | | *Convection Calibration* | | |
| $T_j$ | 0.76 | 0.72 | 1.05 | °C |
| $T_{\text{HFM}}$ | 0.33 | 0.16 | 0.37 | °C |
| $V_{\text{HFM}}$ | 3.92 | 2.48 | 4.63 | μV |
| $V_{\text{RdF}}$ | 3.92 | 3.40 | 5.19 | μV |
| $V_{\text{HTHFS}}$ | 3.92 | 2.49 | 4.64 | μV |
| $S_{\text{HFM}}$ | 10.25 | —— | 10.25 | μV/W/cm² |
| $S_{\text{RdF}}$ | 46.25 | —— | 46.25 | μV/W/cm² |

**Table 4 Average total uncertainties in sensitivity for conduction and convection**

| | Conduction | | |
|---|---|---|---|
| Series no. | $S_t$, μV/W/cm² | $U_{s_t}$, μV/W/cm² | $U_{s_t}$, % |
| | *Conduction* | | |
| 1 | 627.9 | 32.9 | 5.2 |
| 2 | 626.5 | 32.8 | 5.2 |
| 3 | 613.7 | 32.2 | 5.2 |
| 4 | —— | —— | —— |
| | *Convection* | | |
| 1 | 574.7 | 28.9 | 5.0 |
| 2 | 580.9 | 29.9 | 5.1 |
| 3 | 577.2 | 29.1 | 5.1 |
| 4 | 584.3 | 29.6 | 5.1 |

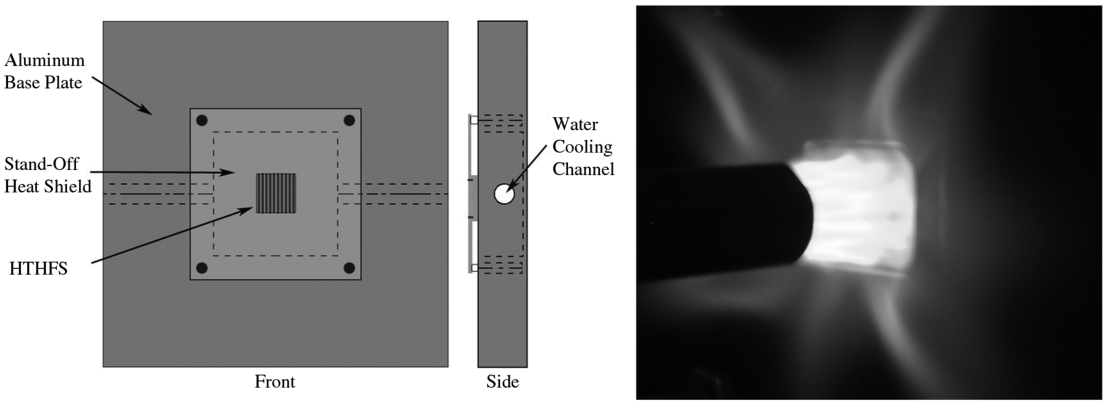


**Fig. 8 Propane torch test apparatus and torch testing.**

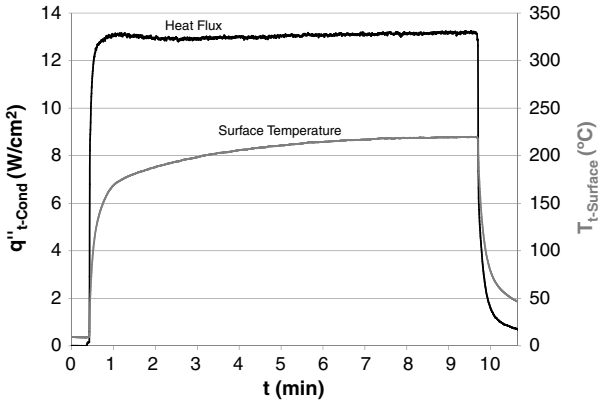


**Fig. 9 Example of torch testing data.**

either calibration approach is associated with the bias error of the reference sensor sensitivity.

## V. Thermal Cycling: Kiln and Torch Tests

As mentioned in Sec. IV, the HTHFS sensor was subjected to repeated thermal cycling to determine the effects on sensor sensitivity and to show conclusively that the HTHFS design can withstand both high temperature and heat flux for an extended period of time. In the first series of tests, the HTHFS was cycled on five successive occasions in air between 100 and 1050°C inside a temperature-controlled kiln. The temperature ramp-up rate ranged from 0.5 to 1.1°C/s. The sensor was allowed to soak at the maximum temperature for 20 min before being pulled out of the kiln for rapid cooling back to a nominal 100°C. The HTHFS performed excellently in these tests and, as shown previously, the sensitivity was unaffected. The effect of thermal expansion mismatch between the two thermoelectric alloys and the insulation was not significant over the temperature range studied. This is evidenced by the fact that no weld failures or cracking of insulation were noted during careful examination of the sensor after thermal cycling. Minimal thermal stress can be expected within the thermopile, because the linear coefficients of thermal expansion are similar for type-K thermocouple materials [9]. Finally, degradation of the insulation material was minor and little-to-no oxidation was observed on the exposed metallic portions of the sensor surface.

A series of propane torch tests reinforced the positive results from the kiln thermal cycling studies. To maximize the applied temperature gradient (and hence the heat flux and thermal stress on the sensor), a water-cooled plate was constructed, as shown in Fig. 8a. The HTHFS was pressed against the surface of the water-cooled plate by a standoff metal shield. Torch applications lasted 10 min and were repeated 15 times without sensor failure. Figure 8b shows a photograph of the HTHFS being subjected to the propane torch. A typical plot of surface temperature and the corresponding heat flux measured by the HTHFS are shown in Fig. 9. Maximum heat flux levels were in the vicinity of 10–13 $W/cm^2$ over the course of testing.

## VI. Conclusions

The HTHFS was successfully prototyped using high-temperature thermoelectric elements and insulators in a durable thermopile design. Calibration of a representative sensor was performed in both conduction and convection heat transfer. Experimental sensitivities near room temperature were very close to the value predicted using simple analysis and a 1-D thermal-resistance model of the sensor. The HTHFS sensor was subjected to numerous thermal cycling tests involving kiln firing and propane torch applications. The sensor's robust construction withstood these tests and calibrations of this sensor after thermal cycling revealed no appreciable shift in sensitivity.

Research efforts are currently focused on a number of HTHFS design and calibration issues. First, the miniaturization of the HTHFS and housing are being studied for increased time response. Higher-temperature thermoelectric alloys are also being considered to increase the maximum operating temperature to above 1500°C. Efforts are underway to develop a high-temperature high-heat-flux radiation calibration facility that will be used to account for temperature-dependent material properties and to determine the HTHFS sensitivity across the operational range.

## Acknowledgments

Funding for this work was provided by Sandia National Laboratories through program managers Jim Nakos and Tom Blanchat. We would also like to acknowledge the support of NASA Dryden Flight Research Center through Tao of Systems Integration, Inc., and NASA contract monitor Larry Hudson. Finally, we wish to thank Virginia Polytechnic Institute and State University student James Sracic for invaluable assistance.

## References

[1] Diller, T. E., *The Measurement, Instrumentation and Sensors Handbook*, edited by J. G. Webster, CRC Press, Boca Raton, FL, 1999, pp. 34.1–34.15.

[2] Raphael-Mabel, S., Huxtable, S., Gifford, A., and Diller, T. E., "Design and Calibration of a Novel High Temperature Heat Flux Gage," American Society of Mechanical Engineers, Paper 2005-72761, July 2005.

[3] *ASM Ready Reference: Thermal Properties of Metals*, Material Data Series, edited by F. Cverna, ASM International, Materials Park, OH, 2002.

[4] Kinzie, P. A., *Thermocouple Temperature Measurement*, Wiley, New York, 1973.

[5] *Manual on the Use of Thermocouples in Temperature Measurement*, American Society for Testing and Materials, Philadelphia, 1970.

[6] Hager, N., "Thin Foil Heat Meter," *Review of Scientific Instruments*, Vol. 36, No. 11, Nov. 1965, pp. 1564–1570. doi:10.1063/1.1719394
[7] Gifford, A., Hoffie, A., Diller, T., and Huxtable, S., "Convection Calibration of Schmidt-Boelter Heat Flux Gages in Shear and Stagnation Air Flow," *Journal of Heat Transfer* (to be published).
[8] Coleman, H. W., and Steele, W. G., *Experimentation and Uncertainty Analysis for Engineers*, Wiley, New York, 1989.
[9] *MatWeb Material Property Data* [online database], http://www.matweb.com [retrieved 1 Dec. 2008].